

**Supplementary Information for:**

## **Direct-write Printing of a Self-Insulating Liquid Metal-Silicone Composite**

Taylor V. Neumann,<sup>a</sup> Emily G. Facchine,<sup>a</sup> Brian Leonardo,<sup>a</sup> Saad Khan<sup>a</sup> and Michael D. Dickey<sup>a,\*</sup>

## Comparison to Einstein's Equation for Hard-Spheres

The traditional Einstein's equation for hard-spheres predicts the increase in viscosity for a fluid with inclusion to follow the trend defined by the first two terms in Equation S1. We have used a modified Einstein equation which takes into account interaction between particles via the quadratic term<sup>1</sup> to account for our higher volume fractions (>1%).

$$\eta = \eta_0(1 + 2.5\phi + 6.2\phi^2) \quad [S1]$$

In this equation,  $\eta$  is the viscosity of the composite material,  $\eta_0$  is the viscosity of the pure fluid, and  $\phi$  is the volume fraction of particles in the fluid. Experimental measurements of the zero-shear viscosity for LMEs are shown in Table S1, and compared to that calculated using Equation S1. We find the viscosities of the LMEs to be greater than the theoretically predicted values, indicating that the EGaln inclusions are not behaving as hard-spheres.

**Table S1.** Comparison of experimental zero-shear viscosity for LMEs with the zero-shear viscosity predicted by the modified Einstein's equation for hard spheres.

EGaln Weight %	EGaln Volume %	Calculated Viscosity (Pa.s)	Experimental Viscosity (Pa.s)
0	0	2.6	2.6
30	6.5	3.09	3.51
50	14	3.83	6.49
70	27	5.53	>12

## Yield Stress & Shear Dependent Viscosity Fitting

The yield stress of the LME follows a Herschel-Bulkley model, defined by the following equation

$$\tau = \tau_0 + k\dot{\gamma}^n \quad [S2]$$

which may be rearranged to describe the viscosity (shear stress divided by the shear rate) in the following manner

$$\eta = \tau_0(\dot{\gamma})^{-1} + k(\dot{\gamma})^{n-1} \quad [S3]$$

where  $\eta$  denotes the viscosity,  $\dot{\gamma}$  is the shear rate,  $\tau_0$  is the yield stress, and  $K$  and  $n$  are fitting parameters. Note that a value of  $n = 1$  and  $\tau_0 = 0$  represents a Newtonian fluid, which matches the behavior of Sylgard 184. Table S2 reports values used to produce a "best-fit" curve of the LME samples at each concentration, fit to Equation S3. These correspond to the curves shown as dashed lines in **Figure 2a**.

**Table S2.** LME Power-law Model Fitting Parameters

EGain Concentration	Flow Index (n)	Consistency Index (K)	Yield Stress (Pa)
0 wt.%	1	2.63	0
30 wt.%	0.99	3.09	0
50 wt.%	0.92	5.91	0.0044 (negligible)
70 wt.%	0.81	12.4	2.5
80 wt.%	0.75	21.9	18.9
90 wt.%	0.54	78.75	70.7

### Graphically Estimating Yield Stress

The yield stress may be estimated graphically by the plateau of stress values as shear rates approach zero. This plateau is shown in **Figure S1** for 80 and 90 wt.% LME samples. These exhibit a yield stress of  $16.2 \pm \text{Pa}$  and  $64.2 \text{ Pa}$ , respectively. These are fit to Equation S2. The values are comparable values to those found via fitting Equation S3 above (see Table S1) within an error of  $\pm 6\%$ . Such measurement variation in yield stress is well within the accepted norm.<sup>2</sup>

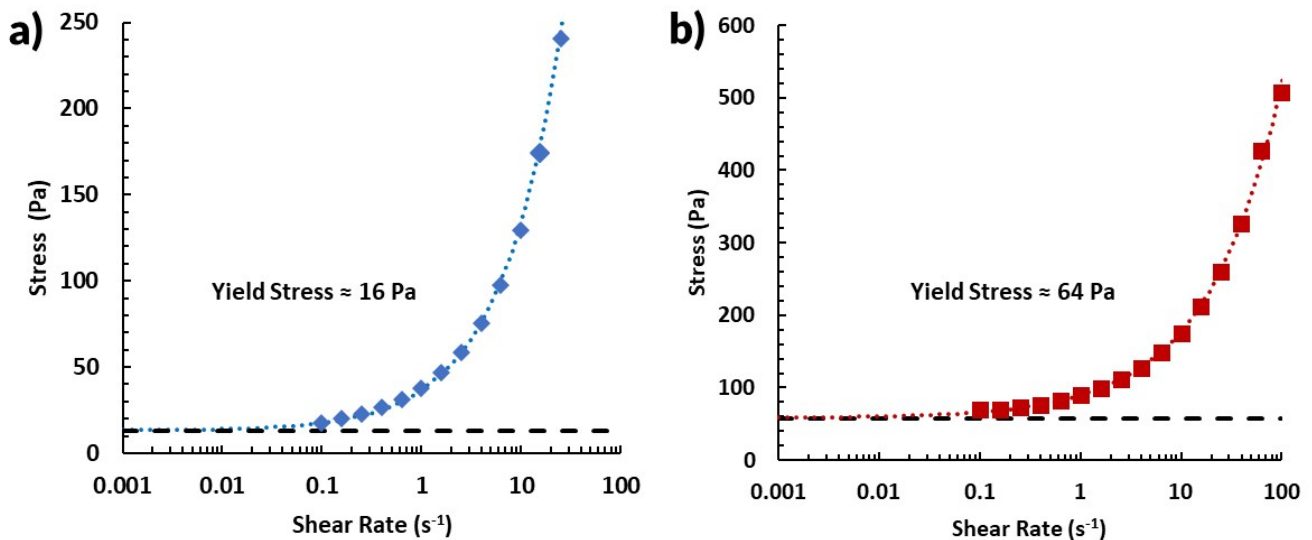


**Figure S1.** Plot of stress vs shear rate (a) 80 wt.% and (b) 90 wt.% LME. Yield stress is taken where the plateau of stress occurs. For 80 wt.%, the yield stress is  $\sim 16 \text{ Pa}$ , and for 90 wt.%, the yield stress is  $\sim 64 \text{ Pa}$ .

## Measuring LME Particle Size

The particles were imaged using an optical microscope and then measured via using ImageJ. An example of the imaged particles is shown below. Particle radius is calculated by assuming a spherical particle.

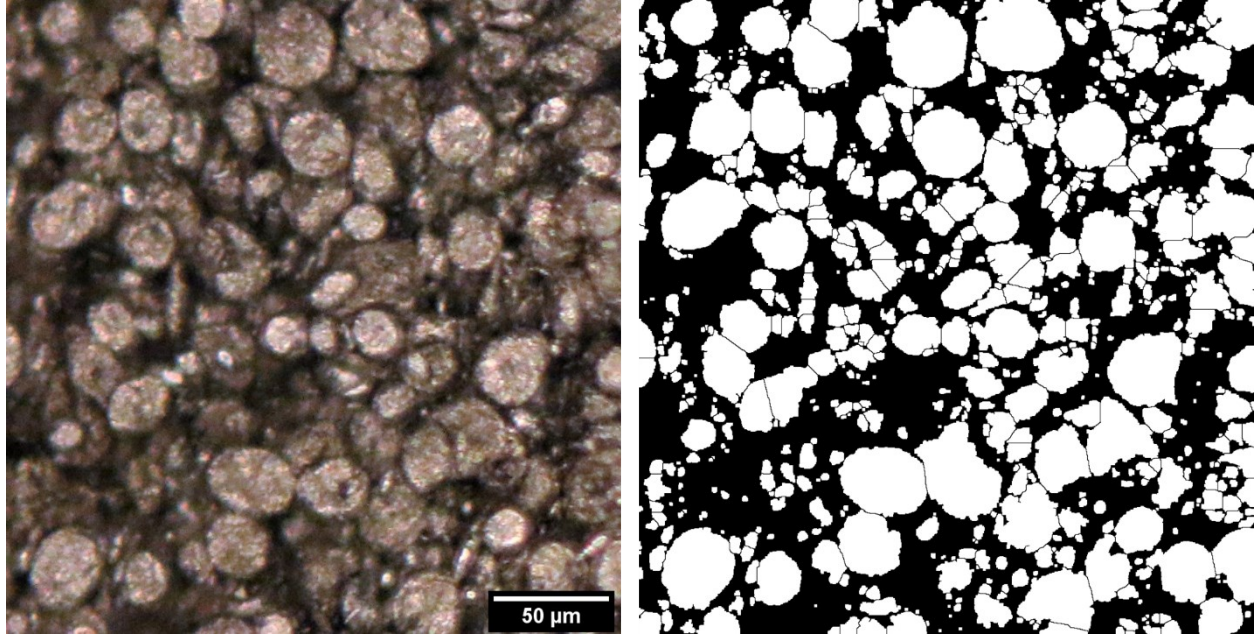


**Figure S2.** An optical micrograph of particles in a cast film of 90wt% LME, taken in transmission mode, and the resulting particles measured by ImageJ.

## Particle Settling Rates

Assuming that particles undergo Stokes' flow while settling, we arrive at the following equations.

$$v(t) = v_T(1 - e^{-t/\tau}) \quad [S4]$$

$$v_T = \frac{2(\rho_{LM} - \rho_{PDMS})}{9\mu}gr^2 \quad [S5]$$

$$\tau = \frac{2(\rho_{LM} - \rho_{PDMS})}{9\mu}r^2 \quad [S6]$$

From the above equations, we see that as time ( $t$ ) goes to infinity, the value of the term  $e^{-t/\tau}$  approaches zero, which drives the velocity,  $v(t)$ , to approach the terminal velocity,  $v_T$ . Equation S7 can be used to determine the time at which the particle reaches 95% of the terminal velocity is defined by

$$t = -\tau \ln\left(\frac{r_0}{r}\right)(0.95) \quad [S7]$$

We will take the viscosity of pure PDMS (2.63 Pa.s) for consideration here. Clearly,  $\tau$  increases with the square of particle radius per Equation S6, thus larger particles will fall the faster than smaller particles. For the largest particles of interest here (radius of 118  $\mu\text{m}$ ), the time to reach 95% of terminal velocity is 3.75 s. For our system, the particle settling takes place on a time scale much greater than this ( $\sim$ hours), and therefore we can safely assume that the particles all fall at their terminal velocity, although the ultimate analysis is complicated by the effect of particles on viscosity.

To confirm the assumptions for Stokes' flow, we checked if the initial velocity of the interface was proportional to the radius squared ( $r^2$ ), as discussed above. The initial velocity of the particles should approximate Stokes flow, as that is before particles may form flocs or sediment and limit further motion. If the vessel was infinitely tall, we would expect this behavior to continue. **Figure S4** shows how the experimentally measured initial velocity compares to the Stokes law predicted velocity from Equation S5.

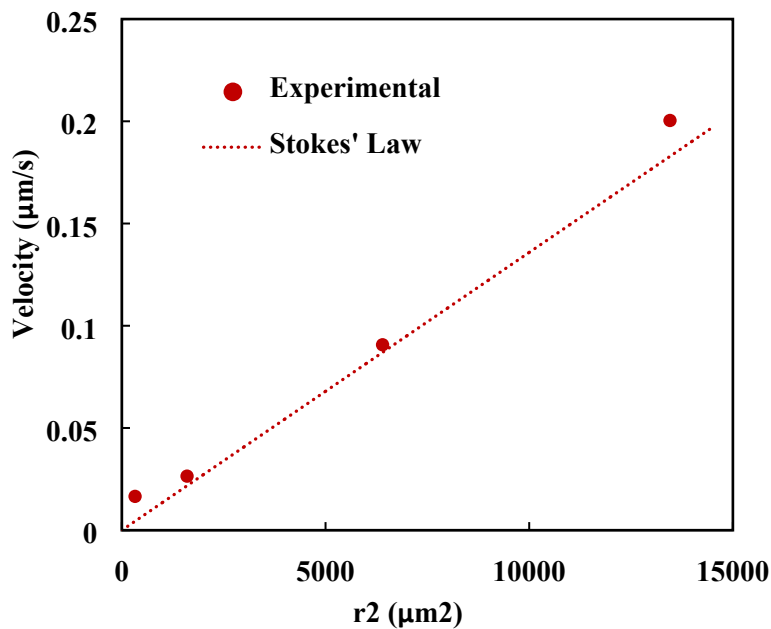


**Figure S3.** Plot showing the linear relation between the initial velocity and particle radius squared. The line follows the behavior predicted by Equation S5, and is compared to the experimentally measured velocity.

#### Fitting of the Sedimentation Interface Position

The position of the interface between EGaIn rich and EGaIn depleted zones (shown in the main text **Figure 4**, measured as the distance from the air-liquid interface to the interface between the

rich/depleted zones) can be fit to an exponential function with respect to time (or time multiplied by the dimensionless Archimedes' number). The empirically derived equations are given below.

For the size specific curves, the equation would follow the form

$$z = A + Be^{-t/C} \quad [S8]$$

Where  $z$  is the position of the interface,  $t$  is time, and  $A$ ,  $B$ , and  $C$  are fitting parameters. For the composite curve which is independent of particle size the equation would follow the form

$$z = A + Be^{-Ar * t/C} \quad [S9]$$

Where  $Ar$  is the Archimedes' number. **Table S3** below summarizes the values of  $A$ ,  $B$ , and  $C$  for each case discussed.

**Table S3.** Sedimentation Front Position Fitting Parameters

Particle Size	Fitting Parameters		
	A	B	C
116 $\mu\text{m}$	0.33381	0.66048	134.3841
80 $\mu\text{m}$	0.42415	0.56655	322.9361
40 $\mu\text{m}$	0.83235	0.14787	344.7493
18 $\mu\text{m}$	0.89374	0.09637	254.8299
Composite Curve	0.34968	0.61543	0.10874

### Rheology Experimental Steps

All the rheology experiments were conducted using a rheometer equipped with a parallel plate geometry (TA Instruments AR-G2) at a gap height of 1000  $\mu\text{m}$ .

Initial Tests (Conducted for all samples from 0 to 90 wt.% EGaln)

1. Frequency Sweep at 2% strain from 0.1 to 100.0 rad/s.
2. Flow Sweep from a shear rate of 0.1  $\text{s}^{-1}$  to 100.0  $\text{s}^{-1}$ .
3. Flow Sweep from a shear rate of 100.0  $\text{s}^{-1}$  to 0.1  $\text{s}^{-1}$ .
4. Oscillatory Amplitude Sweep at a frequency of 10.0 rad/s from strain of 0.2 to 20%.

Structure Recovery Tests (Only conducted using 90 wt.% EGaln)

1. Flow Sweep from shear rate of 0.1  $\text{s}^{-1}$  to 100.0  $\text{s}^{-1}$ .
2. Oscillatory Amplitude Sweep at a frequency of 10.0 rad/s from strain of 0.2 to 20%.

3. Time Sweep for 500 s at 1.0% strain and angular frequency of 1.0 rad/s.
4. Time Sweep for 500 s at 100% strain and angular frequency of 1.0 rad/s.
5. Repeat steps 3 and 4 for multiple cycles to confirm structure recovery.

## 3D Printing Setup



**Figure S4.** The 3D printing stage. Syringe barrels full of ink are loaded into the white plastic clip to be printed. Extrusion is driven by the Nordson Ultimius V pressure actuator (out of frame).

## References

- 1 C. W. Macosko, *Rheology: Principles, Measurements, and Applications*, Wiley-VCH, 1st edn., 1994.
- 2 H. J. Walls, S. B. Caines, A. M. Sanchez and S. A. Khan, *Journal of Rheology*, 2003, **47**, 847–868.



## Supporting Videos

**Video S1** – LME droplet spreading. A comparison of the spreading of individually dispensed droplets of 30, 50, and 80 wt% LME, showing the lower concentrations flow outward while the higher concentration holds its shape.

**Video S2** – 3D printing of multilayer structures. A video showing printing of single- and multi-layer features using 90 wt% LME printed through a 20 gauge nozzle. These videos are sped up to 2x real time.

**Video S3** – Peeling to induce conductivity. A single LME line (90 wt% EGaIn) is peeled from a glass slide and the conductivity is measured using a multimeter. The top of the feature remains insulating.

**Video S4** – Demonstration of biphasic conductor. The self-insulating printed LME feature has been printed using 90 wt% LME, and then peeled from a glass slide, inducing conductivity. If the LME is placed with the conductive face downward, the LED is illuminated.